International Journal of Control, Automation, and Systems (2009) 7(4):553-565 http://www.springer.com/12555
DOI 10.1007/s12555-009-0407-1

Proportional Navigation-Based Collision Avoidance for UAVs

Su-Cheol Han, Hyochoong Bang*, and Chang-Sun Yoo

Abstract: A collision avoidance algorithm for unmanned aerial vehicles (UAVs) based on the conventional proportional navigation (PN) guidance law is investigated. The proportional navigation guidance law being applied to a wide range of missile guidance problems is tailored to the collision avoidance of UAVs. This can be accomplished by guiding the relative velocity vector of the aircraft to a vector connecting the current aircraft position to the safety boundary of the target aircraft. Stability of the proposed algorithm is also studied using the circle criterion. The stability condition can be established by choosing the navigation coefficient within a certain bound. The guidance law is extended to 3-dimensional maneuver problems. Inherent simplicity and robustness of the PN guidance law provides satisfactory collision avoidance performance with different initial conditions.

Keywords: Collision avoidance, proportional navigation, stability, 3-dimensional problem, unmanned aerial vehicles.

1. INTRODUCTION

Aircraft collision is a serious concern as the number of aircraft in operation increases. Therefore, further demand on ground air traffic control workload is expected. So far, most air traffic controls are operated by ground station command centres whose staffs play a key role in the safe operation of air traffic. In particular, UAVs (Unmanned Aerial Vehicles) will add to the volume of aircraft needing consideration to ensure increased collisions are avoided in the future. In the future, autonomous UAVs are expected to carry sophisticated avoidance systems when flying together with conventional aircraft. Onboard sensor systems combined with self-operating algorithms will ensure collision avoidance with little intervention from ground stations.

With the rapid increase in air traffic in the near future, ground station-based air traffic control may not be sufficient to safely handle all aircraft. Thus, self-contained onboard air traffic control or collision avoidance systems are under intensive research. For autonomy of collision avoidance, avoidance laws for multiple aircraft in operation are needed. For instance, onboard sensors can detect other aircraft nearby. Information related to the target aircraft such as position, velocity, and heading angle can be used to build an avoidance command. This architecture is close to a feedback control approach. The avoidance law should be generated in real-time, and simple to implement.

Many collision avoidance laws were also proposed for applications in the area of robotics. Katib proposed the potential field-based approach for avoidance law design [1]. A series of follow-on research has been conducted, motivated by the potential filed technique. The fuzzy logic algorithm was proposed by Tang *et al.* for a robot soccer problem [2]. Rathbun *et al.* applied the genetic algorithm [3] and Tomlin *et al.* worked on the hybrid system approach [4] for collision avoidance. Moreover, Sigurd and How applied the total field approach to construct an avoidance algorithm [5].

Collision avoidance for UAVs has received intensive focus recently. Ryan *et al.* presented an overview of cooperative UAV control research [6]. Ghose *et al.* studied a collision cone based UAV collision avoidance algorithm [7]. Other research works on collision avoidance are reported from [8] to [10]. How *et al.* showed flight demonstrations for cooperative control of multiple UAVs [11].

In this study, a collision avoidance law based upon conventional PN (Proportional Navigation) guidance laws is investigated. The PN guidance law is one of the most general strategies for the missile engagement scenario [12]. Plenty of source material regarding PN guidance is available [12-15]. In order to apply the PN guidance law to collision avoidance problems, a collision avoidance vector is first defined, then the vector defining heading angle of the aircraft is guided to the pre-defined collision avoidance vector. Stability analysis of PN-based collision avoidance guidance (PNCAG) using so-called circle criterion is presented to provide a condition for stabilizing the navigation constant. Moreover, the

Manuscript received July 16, 2007; revised October 19, 2008; accepted February 26, 2009. Recommended by Editorial Board member Sangdeok Park under the direction of Editor Hyun Seok Yang. This research was performed for the Smart UAV Development Program, one of 21st Century Frontier R&D Programs funded by the Ministry of Science and Technology of Korea.

Su-Cheol Han is with Korea Airforce, Korea (e-mail: schan@fdcl.kaist.ac.kr).

Hyochoong Bang is with the Department of Aerospace Engineering, Korea Advanced Institute of Science and Technology, 373-1 Kusong-dong, Yusong-gu, Daejeon 305-701, Korea (e-mail: hcbang@ascl.kaist.ac.kr).

Chang-Sun Yoo is with the Smart UAV Development Center of Korea Aerospace Research Institute, Yusong-gu, Daejon 305-333, Korea (e-mail: csyoo@kari.re.kr).

* Corresponding author.

guidance law is extended to 3-dimensional problems. The collision avoidance vector is designed toward 3-dimensional cylinder type safety regions. Altitude constraint is added as an additional variable for the synthesis of 3-dimensional PNCAG law. Geometric analysis is largely used to develop the desired collision avoidance command. In order to prevent relatively unsafe vertical avoidance, a weighting parameter is introduced which provides flexibility in choosing avoidance directions.

The proposed collision avoidance law could be considered as an extension of the conventional PN guidance law for the problem of aircraft collision. The guidance law is designed to steer the aircraft in a flight path toward the boundary of a safety bound. The safety bound is a circle and cylinder with a minimum radius to prevent collision. Thus, the simple modification of the classical PN guidance law can lead to a UAV collision avoidance strategy. The inherent characteristics of the PN are also reflected in the collision avoidance law. Extension to 3-dimensional maneuvers is another attractive feature of the proposed method.

This paper is organized as follows. First, the principal idea of the PNCAG law is introduced. To facilitate understanding of the proposed approach, linear analysis of the PNCAG is followed producing an analytical solution. Next, selection of the stabilizing navigation constant is discussed through stability analysis. A linearized solution is presented in section IV to facilitate understanding of the guidance law. The PNCAG law is generalized to a 3-dimensional case in section VI. Finally, concluding remarks are provided.

2. PN-BASED COLLISION AVOIDANCE GUIDANCE

The main objective of collision avoidance is to maintain a pre-defined safety range between the aircraft and target vehicles or obstacles. Geometric configuration for the collision avoidance problem is presented in Fig. 1. An aircraft is facing a target aircraft classified as an obstacle in a two-dimensional plane. For a collision avoidance algorithm, we apply the PN guidance strategy. It is a proven technology with numerous applications to missile guidance problems. Recently, there have been some related studies using the PN approach for collision avoidance of UAVs [16-18].

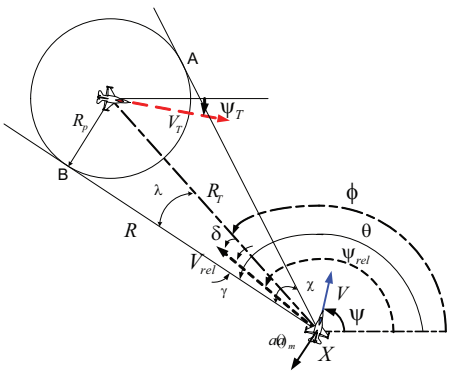

Fig. 1. Geometric configuration fo collision avoidance between two aircraft.

Table 1. Summary of PNCAG algorithm.

```
Do while (Aircraft does not reach the goal)
Calculate the relative velocity vector
 v_rel = v − v_T
   If (Relative velocity vector is out of the obstacle cone)
      Navigation mode is initiated
   Else
      Collision avoidance mode is initiated
   End
End
```

An obstacle cone is defined as a region formed by three points in Fig. 1. The navigation mode is a normal mode for which aircraft fly over a designated course without obstacles. In the collision avoidance mode, the aircraft should perform the collision avoidance maneuver on its route. Based upon the geometry in Fig. 1, a summary on the PNCAG algorithm is presented in Table 1 in a pseudo code.

For collision avoidance, the so-called collision avoidance vector, $\overrightarrow{XB}$ in Fig. 1 is established first. Then the relative velocity vector between the aircraft and the obstacle is steered toward the collision avoidance vector. From Fig. 1, the PN guidance command can be expressed as follows:

$$a = Nv_{rel}\dot{\theta}, \tag{1}$$

where a is input acceleration, $\mathbf{v}_{rel} = \mathbf{v} - \mathbf{v}_T$ is the relative velocity vector between the aircraft and the obstacle, θ represents the direction of collision avoidance, and N is the proportional navigation constant. The avoidance law in (1) is essentially equivalent to the general PN guidance law.

The time rate of change of the collision avoidance vector satisfies

$$\begin{aligned}\dot{\theta} &= \dot{\phi} + \dot{\lambda} \\ &= -\left(\frac{v_{rel}\sin\psi_{rel}}{R_T\cos\phi} + \frac{\dot{R}_T}{R_T}(\tan\phi + \tan\lambda) \right),\end{aligned} \tag{2}$$

where $\tan\lambda = R_p / \sqrt{R_T^2 - R_p^2}$, $sin\phi = (y_T - y)/R_T$ and $cos\phi = (x_T - x)/R_T$ are satisfied. Thus, the PN guidance command can be generated from the information, v_{rel}, ψ_{rel}, R_T, ϕ, λ and $\dot{R}_T$. Derivation of (2) is provided in Appendix A.

3. STABILITY ANALYSIS OF PNCAG

The PNCAG introduced above can be used effectively for the collision avoidance maneuver. Performance of the general PN guidance laws has already been verified in a number of previous studies. In this section, the stability of the PNCAG law is investigated to ensure that the desired collision avoidance is accomplished. The stability analysis of the PN using the circle criterion has

been studied by Gurfil *et al.* [15]. Gurfil assumed that the approaching velocity is a constant, however the approaching velocity of the PNCAG is not a constant in this study. Consequently, some modification is necessary in applying Gurfil's stability analysis method. For stability analysis, Fig. 1 is employed to define the necessary variables.

In Fig. 1, the equation of the motion of the aircraft about the radial direction in the polar coordinate system is derived as

$$R\ddot{\theta} + 2\dot{R}\dot{\theta} = -a_m \cos\gamma = -a, \tag{3}$$

where each parameter is defined in Fig. 1. The approaching velocity $v_c(t)$ and average approaching velocity $\overline{v}_c(t)$ are expressed as

$$v_c(t) = v_{rel}\cos\gamma + R_p\dot{\theta}, \tag{4}$$

$$\overline{v}_c = v_{rel}\Gamma, \tag{5}$$

where R_p is defined in Fig. 1, and

$$\Gamma = \left[1 - \frac{\gamma_0^2 + \gamma_f^2}{15} + \frac{\gamma_0\gamma_f}{30} + \frac{\gamma_0^4 + \gamma_f^4}{420} - \frac{\gamma_0\gamma_f(\gamma_0^4 + \gamma_f^4 - \gamma_0\gamma_f)}{840} + \frac{R_p}{R(N-1)}(\gamma_0 - \gamma_f)\right].$$

Derivation of (5) is presented in the forthcoming Section 4.2. Assuming γ is very small, the approaching velocity is expressed as

$$v_c(t) = v_{rel}\left[1 - R_p\frac{2\gamma_0 + 4\gamma_f}{R_0(N-1)}\right] + 6v_{rel}R_p\frac{\gamma_0 + \gamma_f}{R_0^2(N-1)}\overline{v}_c t_{go}. \tag{6}$$

Let $G(s)$ denote a transfer function from command acceleration to real acceleration. Then the equation of motion has changed form as

$$\ddot{\theta} = \left[c_1 + \frac{c_2}{t_{go}}\right][2 - Ng(t)]\dot{\theta}, \tag{7}$$

where

$$c_1 = 6v_{rel}R_p\frac{\gamma_0 + \gamma_f}{R_0^2(N-1)},\quad c_2 = \frac{1}{\Gamma}\left[1 - \frac{R_p(2\gamma_0 + 4\gamma_f)}{R_0(N-1)}\right],$$

$$L[g(t)] = G(s).$$

And L represents the Laplace operator. The equation of motion is divided into a time invariant part $H(s)$ and the time varying gain $f(x,t)$ such that

$$H(s) = \frac{1}{s}[NG(s) - 2], \tag{8}$$

$$f(x,t) = c_1 + \frac{c_2}{t_{go}}. \tag{9}$$

To apply the circle criterion [19], it is necessary to prove that $c_1 + c_2/t_{go}$ is positive for $t_{go} \in [0, t_f]$. One can see that $c_1 + c_2/t_{go}$ is positive when the navigation constant N is greater than 1.5. Detailed proof on this statement is presented in Appendix B.

Now we apply the circle criterion [20] to the above equation in the region $k \in [\alpha, \beta] = [c_1 + c_2/t_f,\ c_1 + c_2/t_{go}^*]$, where t_{go}^* is the minimum time for which stability is achieved. Then the characteristic equation of the closed-loop system is expressed as

$$1 + kH(s) = 1 + \frac{k}{s}[NG(s) - 2] = 0 \tag{10}$$

or

$$s + k[NG(s) - 2] = 0. \tag{11}$$

If the acceleration command system is set to be a simple first-order system such that $G(s) = a(s)/a_c(s) = 1/(\tau s + 1)$ with $\tau > 0$ as a time constant, then the characteristic equation can be rewritten as

$$\tau t_{go}s^2 + [(1 - 2c_1\tau)t_{go} - 2c_2\tau]s + (N-2)(c_1 t_{go} + c_2) = 0. \tag{12}$$

The sufficient conditions for the stability in the region $t_{go} \in [t_{go}^*, t_f]$ are given by

$$N > 2, \quad t_{go} > 2\frac{c_2\tau}{1 - 2c_1\tau}. \tag{13}$$

Therefore, for system stability using the PNCAG law, the navigation constant N must be greater than 2. Note that if the actuator dynamics are so fast that τ is close to zero, the system is still stable when $N > 2$. The actuator dynamics $G(s)$ is assumed as a first-order system for stability analysis.

4. LINEAR ANALYSIS OF PNCAG

4.1. Linearized PNCAG

In this section, analysis using a linearized system for the PNCAG law is presented. Linearization of the guidance law and associated geometry help us to understand the PNCAG law in detail. Analysis with a linearized system follows Zarchan's approach [21]. First, Fig. 2 is introduced for linearization analysis.

The navigation command is again prescribed by Eq. (1). Furthermore, from the geometry

$$\ddot{x} = -a\cos(\theta - \theta_0) \tag{14}$$

and

$$\frac{x}{R} = \sin(\theta - \theta_0),\ R = \sqrt{R_T^2 - R_p^2}. \tag{15}$$

If $\theta - \theta_0$ is assumed to be small, which is reasonable

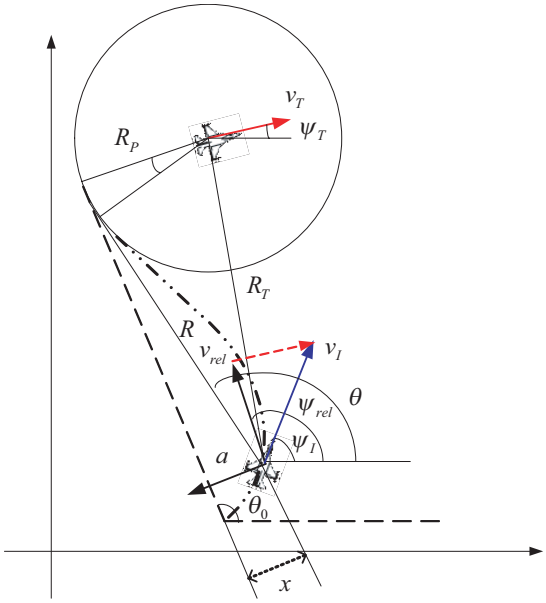

Fig. 2. Geometry for the linearization analysis.

when the two aircraft are initially separated by enough distance, then

$$\ddot{x} = -a, \tag{16}$$

$$\theta = \theta_0 + x/R. \tag{17}$$

Thus one can readily derive

$$\ddot{x} = -a = -Nv_{rel}\dot{\theta} \tag{18}$$

and

$$\dot{x} = -Nv_{rel}\theta + C_1 = -Nv_{rel}(\theta_0 + x/R) + C_1. \tag{19}$$

In other words,

$$\dot{x} + N\frac{x}{t_f - t} = C_1 - Nv_{rel}\theta_0 = C, \tag{20}$$

where C_1 and C are constants to be determined. The solution to Eq. (20) is given by

$$x = e^{-\int_0^t \frac{N}{t_f - T}dT}\{\int_0^t [Ce^{\int_0^\zeta \frac{N}{t_f - T}dT}]d\zeta + C_2\}. \tag{21}$$

Let us consider $x(0) = 0$, and from (21) it follows as $C_2 = 0$. Also, from Fig. 2, $\dot{x}(0) = v_{rel}(\theta_0 - \psi_{rel,0})$ is satisfied. By applying the initial condition $(t = 0)$ to (20), the constant C is, determined as follows:

$$C = \dot{x}(0) = v_{rel}(\theta_0 - \psi_{rel,0}).$$

Solving (21) yields

$$x = \frac{Ct_f}{N-1}\left[1 - \frac{t}{t_f} - (1 - \frac{t}{t_f})^N\right]. \tag{22}$$

Furthermore, the linearized acceleration input can be derived as

$$a = -\ddot{x} = \frac{NC}{t_f}\left[1 - \frac{t}{t_f}\right]^{N-2} \tag{23}$$

together with the velocity

$$\dot{x} = -\frac{NC}{N-1}\left[(1 - \frac{t}{t_f})^{N-1} - 1\right] + C. \tag{24}$$

Therefore, one can see that if the final time t_f is available, then the acceleration command and associated state variables can be derived analytically. Also by using the geometry in Fig. 2

$$\theta = \theta_0 + x/R,$$

$$\dot{\theta} = \frac{\dot{x}}{v_{rel}(t_f - t)} + \frac{x}{v_{rel}(t_f - t)^2}$$

the final form of the acceleration command can be derived as

$$a = N\left[\frac{\dot{x}}{t_f - t} + \frac{x}{(t_f - t)^2}\right]. \tag{27}$$

The acceleration command is a PD (Proportional pulse Derivative) control law over the cross range variable x in Fig. 2.

4.2. Estimation of the final time

In the above analysis, the acceleration command and state variables are formulated in terms of the final time. Thus, estimation of the final time is needed to derive linearized guidance solutions. First, a geometry for the estimation of the final time is presented in Fig. 3.

The trajectory denoted as a dotted line in Fig. 3 allows us to approximate x as a third-order polynomial of the variable z [22]. This is also reasonable enough in the sense that the actual aircraft trajectory is not highly oscillatory in general. Namely,

$$x(z) = d_3z^3 + d_2z^2 + d_1z + d_0. \tag{28}$$

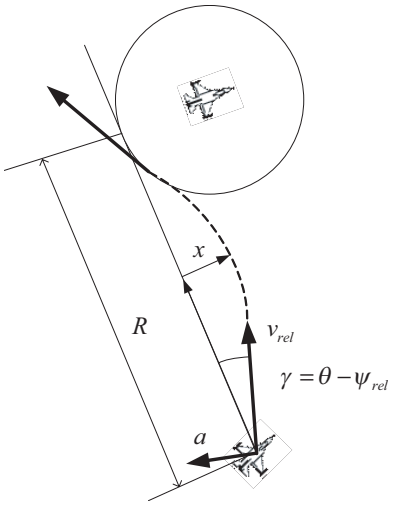

Fig. 3. Variables defined for final time estimation.

Moreover, the angle γ between the collision avoidance and relative velocity vectors satisfies

$$\gamma(z) = \frac{\dot{x}}{v_{rel}} = \frac{\dot{z}}{v_{rel}}(3d_3z^2 + 2d_2z + d_1). \quad (29)$$

If γ is small, then $\dot{z} = v_{rel}$, and (29) can be rewritten as

$$\gamma(z) = 3d_3z^2 + 2d_2z + d_1. \quad (30)$$

Also, the initial and final conditions for x and γ are specified as

$$t = 0, \quad z = 0, \quad \gamma(z) = \gamma_0, \quad x(z) = 0,$$
$$t = t_f, \quad z = R, \quad \gamma(z) = \gamma_f, \quad x(z) = 0.$$

Hence, by making use of the boundary conditions in conjunction with (28) and (30), d_0, d_1, d_2, d_3 are shown to satisfy

$$d_0 = 0, \qquad d_1 = \gamma_0,$$
$$d_1 = -(2\gamma_f + \gamma_0)/R, \qquad d_3 = (\gamma_f + \gamma_0)/R^2.$$

Meanwhile, the approaching velocity v_c is defined as

$$\begin{aligned} v_c &= v_{rel}\cos\gamma(z) + R_P\dot{\theta}(z) \\ &= v_{rel}\cos\gamma(z) - \frac{R_P}{N-1}\dot{\gamma}(z). \end{aligned} \quad (31)$$

Let us represent $\bar{v}_c$ as average approaching velocity over the range, R to be travelled. Then

$$\bar{v}_c = \frac{1}{R}\int_0^R \left[v_{rel}cos\gamma(z) - \frac{R_P}{N-1}\dot{\gamma}(z) \right] dz. \quad (32)$$

By using the Taylor series expansion of the cosine function up to the fourth-order terms

$$cos\gamma(z) \simeq 1 - \frac{\gamma(z)^2}{2!} + \frac{\gamma(z)^4}{4!} \quad (33)$$

the final time can be estimated as

$$t_f = t + \frac{R}{v_{rel}}\left[1 - \frac{\gamma_0^2 + \gamma_f^2}{15} + \frac{\gamma_0\gamma_f}{30} + \frac{\gamma_0^4 + \gamma_f^4}{420} - \frac{\gamma_0\gamma_f(\gamma_0^2 + \gamma_f^2 - \gamma_0\gamma_f)}{80} + \frac{R_p}{R(N-1)}(\gamma_0 - \gamma_f) \right]^{-1},$$

where all necessary parameters are defined already, and γ_0, γ_f are given by

$$\gamma_0 = \theta_0 - \psi_{rel,0},$$
$$\gamma_f = \theta_0 - \psi_{rel,f} = \frac{\theta_0 - \psi_{rel,0}}{1-N},$$

where the subscripts 0, and f denote initial and final states, respectively. (34) provides estimation of the final time when the aircraft crosses the safety boundary point in Fig. 3.

5. SIMULATION

Simulation study is carried out to demonstrate performance of the proposed collision avoidance algorithm. Both nonlinear and linear acceleration commands are examined in the simulation. The aircraft is modelled as a particle in a two-dimensional plane. The obstacle is also assumed to be a particle in the same plane. The corresponding kinematics and dynamic equations of motion for the two-dimensional planar motion are prescribed as

$$\dot{x}(t) = v(t)cos\psi(t), \quad (35)$$
$$\dot{y}(t) = v(t)sin\psi(t) \quad (36)$$

and

$$\dot{v}(t) = -a(t)sin(\psi_{rel}(t) - \psi(t)), \quad (37)$$
$$\dot{\psi}(t) = a(t)cos(\psi_{rel} - \psi(t)), \quad (38)$$

where $v(t)$ and $\psi(t)$ represent the velocity and heading angle of the aircraft, and $\dot{\psi}_{rel}(t) = a(t)/v_{rel}$. The simulation conditions are listed in Tables 2 and 3 for aircraft and obstacles, respectively. Three different initial

Table 2. Simulation conditions for the linear and nonlinear approaches - Aircraft.

	Case I	Case II	Case III
Initial position (km)	(0, 0)	(0, 0)	(0, 0)
Target position (km)	(0, 20)	(0, 20)	(0, 20)
Initial speed (m/s)	100	150	200
Heading angle (rad)	$\pi/2$	$\pi/2$	$\pi/2$

Table 3. Simulation conditions for the linear and nonlinear approaches - Obstacle.

	Case I	Case II	Case III
Initial position (km)	(-10, 10)	(-4.7, 14.,7)	(0, 15)
Target position (km)	(10, 10)	(4.7, 5.3)	(0, 5)
Initial speed (m/s)	100	100	200
Heading angle (rad)	$\pi/2$	$-\pi/4$	$-\pi/2$

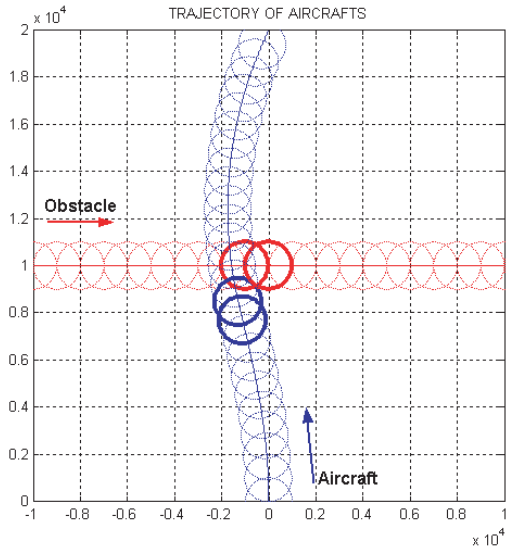

Fig. 4. Simulation results for Case I.

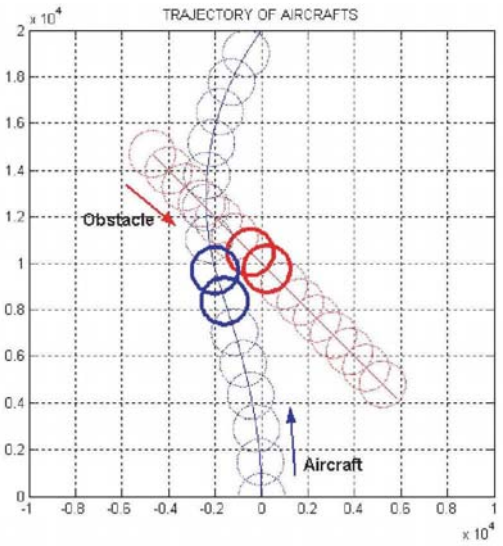

Fig. 5. Response of the simulation results for Case II.

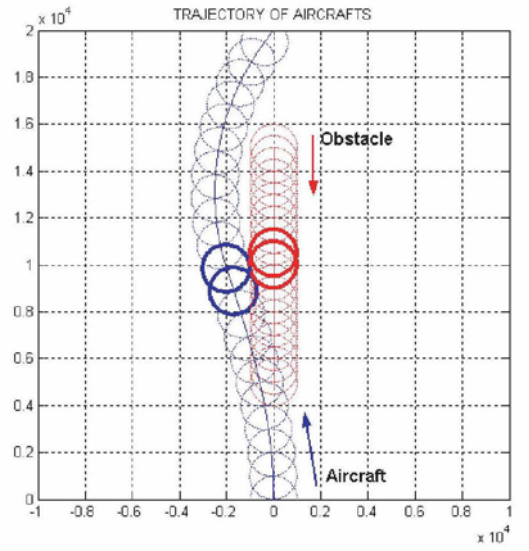

Fig. 6. Simulation results for Case III.

conditions are prescribed for the simulation - Case I, Case II, and CaseIII.

Simulation results for each different initial condition are presented in Figs. 4 to 6. For all cases with different initial conditions, in particular different heading angles, collision avoidance is successfully achieved. The PNCAG law was able to accomplish collision avoidance against a moving obstacle.

6. 3-DIMENSIONAL COLLISION AVOIDANCE

6.1. Collision avoidance for 3-dimensional problem

In this section, the collision avoidance problem formulation is extended to the 3-dimensional flight dynamics and collision models. The safety region is modelled as a cylinder for which the height represents the vertical safety boundary. The collision avoidance course is designed considering the geometry of the cylinder-type safety region. Analysis on the collision course and associated avoidance scenario are conducted also in the context of a PN guidance law.

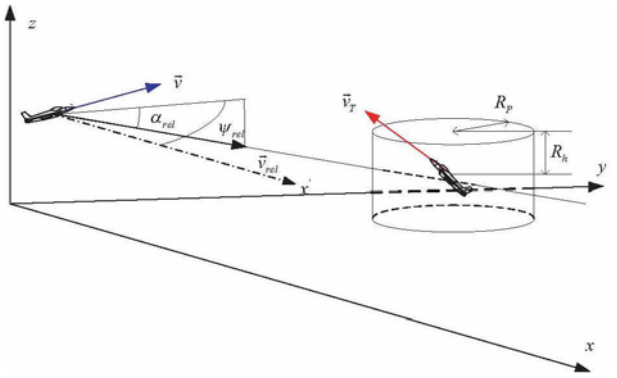

Fig. 7. Collision avoidance problem in the 3-dimensional space.

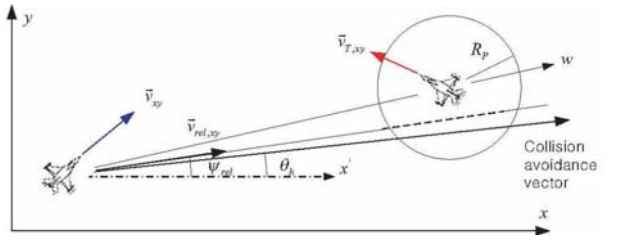

Fig. 8. Two-dimensional view in the $x-y$ plane.

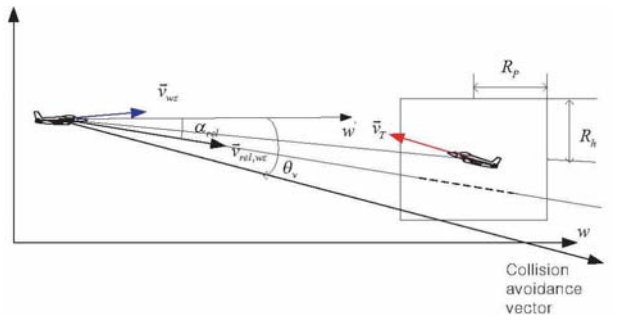

Fig. 9. Two-dimensional view in the $w-z$ plane.

The conflict situation between an aircraft and a target (obstacle) in the 3-dimensional space is illustrated in Fig. 7. For collision avoidance, the safety boundary of the target aircraft is made of a cylinder with a safe height and radius. The exploded view in the two-dimensional $x-y$ and $w-z$ planes are also displayed in Figs. 8 and 9. Consequently, the approaching aircraft should not penetrate the safety region to minimize the possibility of collision. With this goal, the aircraft velocity vector should be steered toward the edge of the cylinder. The acceleration-based command for the 3-dimensional guidance is issued as

$$a_v = Nv_{rel}\dot{\theta}_v, \tag{39}$$

$$a_h = Nv_{rel}\dot{\theta}_h. \tag{40}$$

The above guidance command is a PN guidance command essentially identical to that of the previous two-dimensional case. The vertical (a_v) and horizontal (a_h) acceleration commands consist of angle variables as displayed in Figs. 8 and 9, respectively.

6.2. Determination of the avoidance vector

For the guidance law in (39), (40), the collision avoidance vector should be determined first. For this goal, Fig. 10 shows an exploded view of the collision avoidance vector in the 3-dimensional framework.

From Fig. 10, assuming that the obstacle is detected at a far enough distance, the angle variable satisfies

$$\theta' \simeq r_{BP'} / r_{IB}, \tag{41}$$

where $r_{BP'}$ denotes the range between the points B and P', whereas r_{IB}. for I and B. From now on, the notation r with subscripts is used to denote a range between associated points unless otherwise specified. If we take the time derivative of (41), it follows as

$$\dot{\theta}' = -\dot{r}_{IB}\theta' / r_{IB}. \tag{42}$$

It should be noted that $r_{IB} > 0$ and $\dot{r}_{IB} < 0$, thus $\dot{\theta}' \propto \theta'$. Therefore, the minimum acceleration command is achieved when the collision avoidance vector is selected as a line connecting the points I to P' which minimizes θ'. Furthermore, in order to find the point P' for which θ' becomes a minimum, let us consider the segments $A'D'$, $A''D''$, $A'A''$ and $D'D''$ in Fig. 10.

Case I: $A'A''$ and $D'D''$ sector

First, Fig. 11 shows an additional geometry from the top Fig. 11 to locate the point P'.

In Fig. 11, the following relationships hold

$$\bar{\theta}_L = \phi + \gamma - \psi_{rel}, \tag{43}$$

$$\bar{\theta}_R = -\phi + \gamma + \psi_{rel}, \tag{44}$$

and

$$\delta = \psi_{rel} - \phi. \tag{45}$$

Furthermore,

$$r_{IB} = \bar{R}_T \cos\delta + R_P,$$

where R_p is the radius of the safety cylinder in Fig. 8, and

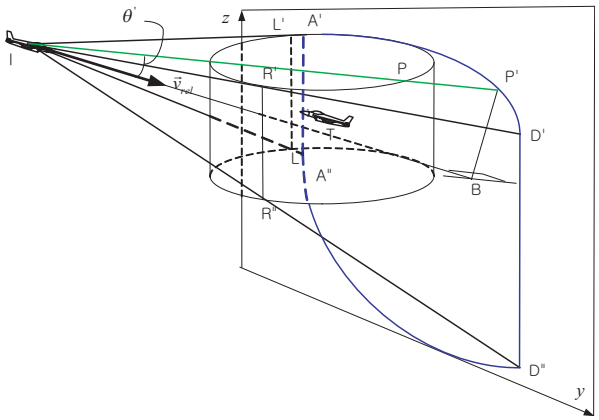

Fig. 10. Exploded view of the 3-dimensional collision avoidance vector.

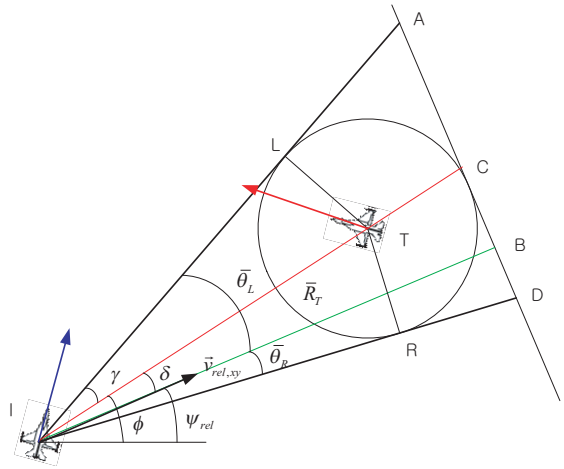

Fig. 11. Additional view for determination of the collision avoidance vector.

the distance from the aircraft to the target is given by $\bar{R}_T = \sqrt{(x-x_T)^2 + (y-y_T)^2}$. Next another auxiliary geometry formed by the points AIB is displayed in Fig. 12. The height of AIB, $r_{LL'}$ can be written as

$$r_{LL'} = \Delta z = z_T + \Delta z_T - z, \quad -R_h \le \Delta z_T \le R_h. \tag{47}$$

Also,

$$r_{IL} = \sqrt{(x-x_T)^2 + (y-y_T)^2 - R_P^2} \tag{48}$$

and

$$r_{IA} = r_{IB} / \cos\bar{\theta}_L. \tag{49}$$

Furthermore, it can be shown that $r_{AA'} = r_{BB'}$ and

$$r_{IB'} = \sqrt{r_{IB}^2 + r_{BB'}^2}, \tag{50}$$

$$r_{AB} = r_{A'B'} = r_{IB}\tan\bar{\theta}_L. \tag{51}$$

Therefore,

$$\theta_L(\Delta z) = \tan^{-1}\frac{r_{A'B'}}{r_{IB'}} = \tan^{-1}\frac{r_{IB}\tan\bar{\theta}_L}{r_{IB}\sqrt{1 + r_{BB'}^2 / r_{IB}^2}}.$$

Since $r_{IB} >> r_{BB'}$ then θ_L can be approximated as

$$\theta_L(\Delta z) \simeq \tan^{-1}(\tan\bar{\theta}_L) = \bar{\theta}_L. \tag{53}$$

The same procedure can be applied to the sector DIB to produce

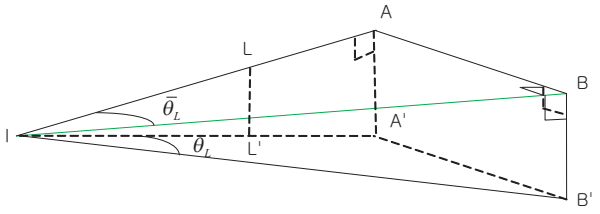

Fig. 12. New geomegtry AIB for the collision avoidance vector.

$$\theta_R(\Delta z) \simeq tan^{-1}(tan\bar{\theta}_R) = \bar{\theta}_R. \tag{54}$$

As a consequence, the arc sectors $A'A''$, $D'D''$ can be considered as near-linear lines. Over the linear lines $A'A''$, $D'D''$, the point for which θ' becomes a minimum can be determined as the point where the point B intersects with $A'A''$, $D'D''$ at 90 degrees.

Case II: $A'D'$, $A''D''$ sector

In order to find the point P' for which the angle θ' becomes minimum over the $A'D'$, $A''D''$ sectors, Fig. 13 is introduced. First, let us note that $-\gamma \le \epsilon \le \gamma$ is satisfied, and ϵ also satisfies

$$\bar{R}^2(\epsilon) - 2\bar{R}_T cos\epsilon \bar{R}(\epsilon) + \bar{R}_T^2 - R_P^2 = 0. \tag{55}$$

The above equation can be solved for the distance $(\bar{R}(\varepsilon))$ to the safety circle as shown in Fig. 13.

$$\bar{R}(\epsilon) = r_{IF} = \bar{R}_T cos(\epsilon) \pm \sqrt{R_P^2 - \bar{R}_T^2 sin^2(\epsilon)}, \tag{56}$$

where the plus sign denotes the semi-circle behind the obstacle whereas the minus sign corresponds to the semi-circle in front of the obstacle.

In Fig. 14, the distance from the aircraft to the projected plane is given by

$$r_{IE} = r_{IB} / cos(\delta - \epsilon) \tag{57}$$

and

$$\begin{aligned} r_{EE'} &= \frac{r_{IE}}{r_{IF}} r_{FF'} = \frac{r_{IB}}{\bar{R}(\epsilon)cos(\delta-\epsilon)}(R_h + z_T - z) r_{EE'}, \\ r_{EE''} &= \frac{r_{IB}}{-R(\epsilon)cos(\delta-\epsilon)}(-R_h + z_T - z). \end{aligned} \tag{58}$$

In order to locate a point which results in the minimum range between points B and P', a parameter $R' = r_{BP'}^2 / r_{IB}^2$ is defined. Then,

$$\begin{aligned} R' &= \frac{r_{BP'}^2}{r_{IB}^2} = \frac{r_{BE'}^2}{r_{IB}^2} . = \frac{r_{EE'}^2 + r_{BE}^2}{r_{IB}^2} \\ &= tan^2(\delta - \epsilon) + \left[\frac{z_T - z \pm R_h}{\bar{R}(\epsilon)cos(\delta\epsilon)} \right]^2 . \end{aligned} \tag{59}$$

Taking the differentiation of (59) with respect to ϵ yields

$$\frac{\partial R'}{\partial \epsilon} = 2 \frac{sin(\delta-\epsilon)\left(1 - \frac{\tilde{z}}{\bar{R}(\epsilon)^2}\right) - cos(\delta-\epsilon)\left(\frac{\tilde{z}^2 \dot{\bar{R}}(\epsilon)}{\bar{R}(\epsilon)}\right)}{cos^3(\delta-\epsilon)}, \tag{60}$$

where $\tilde{z} = z_T - z \pm R$. Since $\bar{R}(\varepsilon) >> |z_T - z \pm R_h|$, then (60) can be rewritten as

$$\frac{\partial R'}{\partial \epsilon} \simeq 2 \frac{sin(\delta-\epsilon)}{cos^3(\delta-\epsilon)} \tag{61}$$

with $\partial^2 R' / \partial \epsilon^2 > 0$. This verifies that when $\epsilon \simeq \delta$, R' becomes a minimum, the range $(r_{BP'})$ between points B and P', is also a minimum.

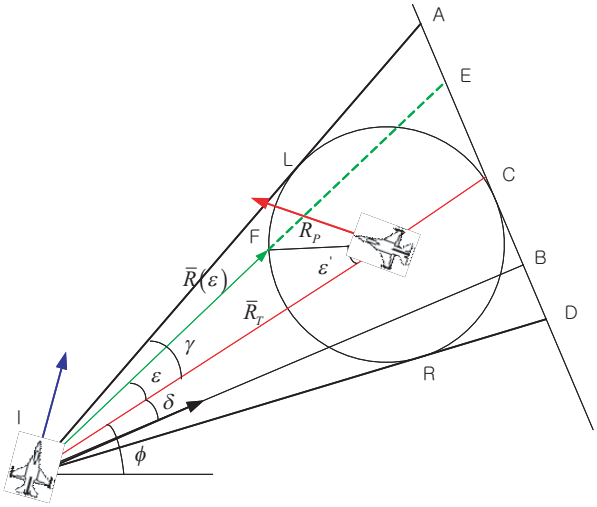

Fig. 13. Two-dimensional view to determine the collision avoidance vector over $A'A''$, $D'D''$ sector.

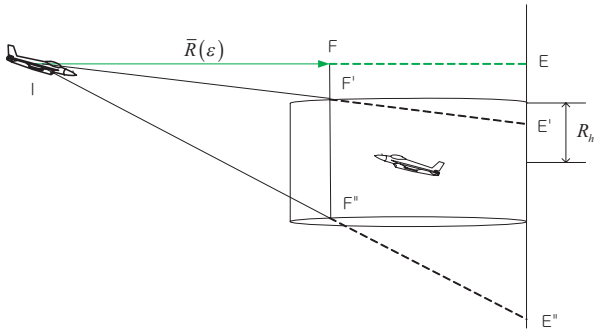

Fig. 14. Side view to determine the collision avoidance vector.

6.3. Vertical maneuver weighting parameters (η_U, η_D)

In general, the safety distance for collision avoidance is much larger in the horizontal plane than the vertical plane. Thus, the collision avoidance vector tends to point in a vertical direction. But in practical cases, the margin for vertical maneuvers by aircraft is very limited compared to horizontal maneuvers. Thus, maneuvering in a vertical direction may be riskier than maneuvering horizontally. This motivates us weighting parameters by which we can artificially create maneuvers in the horizontal direction even if the vertical maneuver is more efficient in terms of energy consumption (47).

The weighting parameters can be determined by several factors. For instance, some ground obstacles and other aircraft should be considered for the weighting factors. Furthermore, aerodynamic characteristics of the

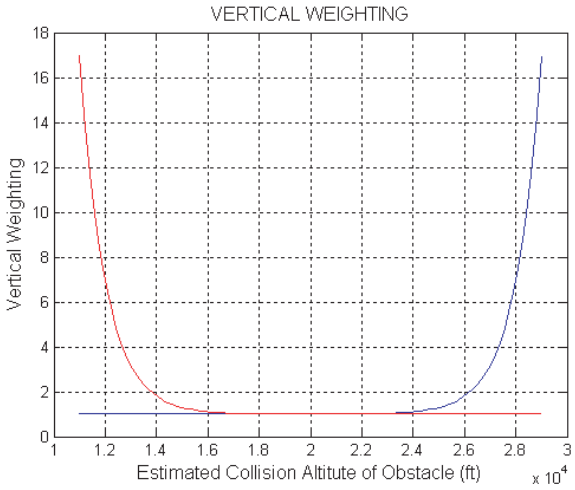

Fig. 15. Trend of the weighting parameters for the vertical maneuver (alt_{min} = 3048m, alt_{max}=9120m).

aircraft could be an important factor to be taken into account. Mathematically, the weighting factor (η) can be modelled in the form

$$\eta = f(alt_{max}, alt_{min}, h_g, c_{aero}, \cdots\cdots), \tag{62}$$

where alt_{max} and alt_{min} represent maximum and minimum operational altitude, respectively, h_g is the height of ground obstacles, and c_{aero} denotes aerodynamic coefficients. In this study, only altitude limitations are considered in the formulation. The weighting parameters for the vertical maneuver are defined as follows:

$$\eta_D = 1 + 16e^{-\frac{alt_{est} - alt_{min} - R_h}{1000}}, \tag{63}$$

$$\eta_U = 1 + 16e^{-\frac{alt_{max} - alt_{est} - R_h}{1000}}, \tag{64}$$

where alt_{est} represents the expected altitude estimate of the obstacle, and can be written as

$$alt_{est} = z_T + \frac{v_{Tz}(R_{Txy}cos\delta - \sqrt{R_P^2 - R_{Txy}^2 sin\delta})}{v_{rel,xy}}, \tag{65}$$

where the variable z_T and v_{Tz} represent the target coordinate and speed in z direction, and the subscript xy denotes $xy-plane$. The weighting parameters with respect to the obstacle altitude are displayed in Fig. 15.

6.4. Computation of $\dot{\theta}_v$

Once the collision avoidance vector is determined, the time derivative of the angle changes $(\dot{\theta}_v, \dot{\theta}_h)$ should be established for the PNCAG law. The basic idea is analogous to the 2-dimensional case, and it is simply extended to the 3-dimensional case as the guidance law in (39) and (40). First, the time derivative of the vertical angle is derived. In Fig. 14, the distance, $\bar{R}(\delta)$, between the aircraft and obstacle is given by

Table 4. Algorithm for determining $\dot{\theta}_v$.

If $z > z_T + R_h$

$\dot{\theta}_v = min[\dot{\theta}_{vUR}, \dot{\theta}_{vDF}]$

elseif $z_T - R_h \le z \le z_T + R_h$

$\dot{\theta}_v = min[\dot{\theta}_{vUF}, \dot{\theta}_{vDF}]$

Else

$\dot{\theta}_v = min[\dot{\theta}_{vUF}, \dot{\theta}_{vDR}]$

where the subscripts U and D correspond to the upper and bottom parts of the cylinder, whereas F and R denote the front and rear sections of the semi-circle.

$$\bar{R}(\delta) = R_{Txy}cos\delta \pm \sqrt{R_P^2 - R_{Txy}^2 sin\delta}, \tag{66}$$

where

$$\delta = \psi_{rel} - sin^{-1}\frac{(y_T - y)}{R_{Txy}} \tag{67}$$

and y, y_T denote y components of the aircraft and target. Furthermore,

$$tan\theta_v = \frac{\Delta z}{\bar{R}(\delta)},\ \Delta z = z_T - z \pm R_h \tag{68}$$

where plus and minus signs represent top and bottom parts of the cylinder, respectively. The time derivative of (68) results in

$$\dot{\theta}_v = \frac{(v_{Tz} - v_z)\bar{R}(\delta) + \Delta z v_{rel,xy}}{\bar{R}^2(\delta) + \Delta z^2}. \tag{69}$$

As is shown in Fig. 14, there are four possibilities in the time derivative of the angle, $\dot{\theta}_v$. The algorithm for determining a particular $\dot{\theta}_v$ out of four is summarized in Table 4.

6.5. Computation of $\dot{\theta}_h$

The time derivative of the horizontal angle θ_h can be computed from

$$\dot{\theta}_h = \dot{\phi} \pm \dot{\gamma}, \tag{70}$$

where

$$\dot{\phi} = -\left[\frac{v_{rel,xy} sin\psi_{rel}}{R_{Txy}cos\phi} + \frac{\dot{R}_{Txy}}{R_{Txy}}tan\phi\right] \tag{71}$$

and

$$\dot{\gamma} = -\frac{\dot{R}_{Txy}}{R_{Txy}}tan\gamma. \tag{72}$$

Collision avoidance direction in the left or right-hand side can be decided as follows; if $\psi_{rel} > \phi$, then

$\dot{\theta}_h = \dot{\phi} + \dot{\gamma}$, and if $\psi_{rel} < \phi$, then $\dot{\theta}_h = \dot{\phi} - \dot{\gamma}$.

The time rate of changes of the vertical and horizontal Angles $(\dot{\theta}_v, \dot{\theta}_h)$ combined with vertical maneuver weighting parameters (η_U, η_D) are derived as follows:

$$\begin{bmatrix} \dot{\theta}_v \\ \dot{\theta}_h \end{bmatrix} = \begin{bmatrix} A & 0 \\ 0 & B \end{bmatrix} \begin{bmatrix} \dot{\theta}_v \\ \dot{\theta}_h \end{bmatrix}, \tag{73}$$

where

$$A = max\left[sign\left(\left\| \dot{\theta}_h \right\| - \left\| \eta \dot{\Theta}_v \right\| \right), 0 \right],$$

$$B = max\left[sign\left(\left\| \eta \dot{\Theta}_v \right\| - \left\| \dot{\theta}_h \right\| \right), 0 \right],$$

$$\eta = \begin{bmatrix} \eta_U & \eta_U & \eta_D & \eta_D \end{bmatrix},$$

$$\dot{\Theta}_v = \begin{bmatrix} sign\left(\left\| \dot{\theta}_v \right\| - \left\| \dot{\theta}_{vUF} \right\| \right) + 1 \\ sign\left(\left\| \dot{\theta}_v \right\| - \left\| \dot{\theta}_{vUR} \right\| \right) + 1 \\ sign\left(\left\| \dot{\theta}_v \right\| - \left\| \dot{\theta}_{vDF} \right\| \right) + 1 \\ sign\left(\left\| \dot{\theta}_v \right\| - \left\| \dot{\theta}_{vDR} \right\| \right) + 1 \end{bmatrix} \dot{\theta}_v$$

and $sign(\,)$ denotes the signum function. The time rate of changes of the vertical and horizontal angles $(\dot{\theta}_v, \dot{\theta}_h)$ for the collision avoidance vector can be directly incorporated into the 3-dimensional PNCAG guidance command in (39) and (40).

To verify the proposed algorithm, a simulation study with different initial conditions is performed with the conditions in Tables 5 and 6, respectively.

Simulations are also conducted with different weighting parameters for the vertical maneuver. First Fig. 16 shows a 3-dimensional collision avoidance scenario for the Case I initial condition. Collision avoidance takes place about the vertical direction. Fig. 17 presents simulation results for Case I but with different design parameters in altitude limits as well as weighting parameters. As we can see, collision avoidance is

Table 5. Simulation condition for 3-dimensional collision avoidance (aircraft).

	Case I	Case II
Initial position (km)	(0,0,5.49)	(0,0,5.49)
Target position (km)	(0, 74.03, 4.31)	(0,74.03, 4.31)
Initial speed (m/s)	102.7	102.7
Heading angle (rad)	$-\pi/2$	$\pi/2$
Flight path angle(rad)	-0.0165	-0.0165

Table 6. Simulation conditions for the linear and nonlinear approaches (obstacle).

	Case I	Case II
Initial position (km)	(-47.22,37.04,4.88)	(0,74.03,4.88)
Target position (km)	(28.85, 37.04, 4.88)	(0,0, 4.88)
Initial speed (m/s)	102.7	102.7
Heading angle (rad)	0	$-\pi/2$
Flight path angle (rad)	0	0

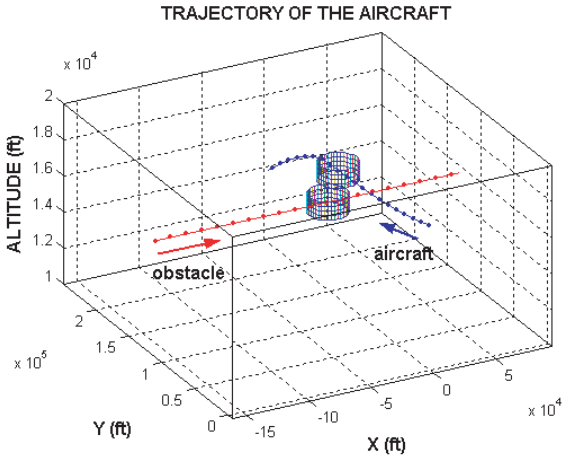

Fig. 16. 3-dimensional simulation results for Case I ($alt_{max} = 6080m$, $alt_{min} = 3048m$, $\eta_U = 1.7966$, $\eta_D = 1.1078$).

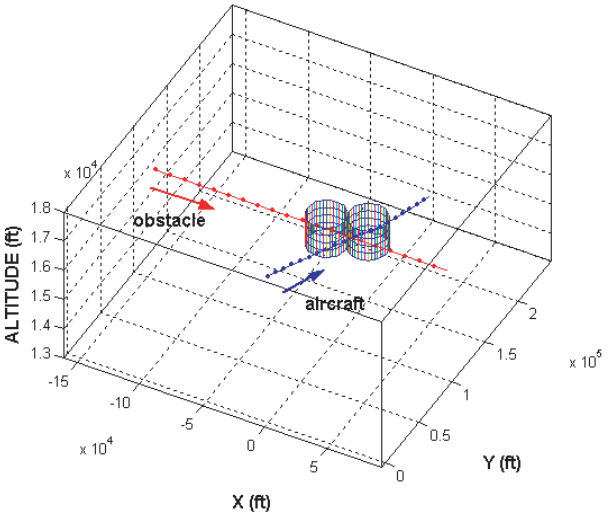

Fig. 17. 3-dimensional simulation results for Case I ($alt_{max} = 5486m$, $alt_{min} = 3962m$, $\eta_U = 6.8861$, $\eta_D = 3.1654$).

achieved in the horizontal direction. It is significantly different from that of Fig. 16 where the aircraft avoids collision in the vertical direction. This illustrates again the effectiveness of weighting parameters in designing the desired avoidance maneuvers.

In Fig. 18, the simulation result for Case II is illustrated with appropriate design parameters. The aircraft and obstacle approach each other from opposite directions. In this case, collision avoidance also takes place in the vertical direction. Fig. 19 also shows simulation results for Case II. With different weighting parameters, especially large η_U, η_D, the collision avoidance vector is steered in the horizontal plane. This again illustrates the effectiveness of the weighting parameter.

Through the simulation results, 3-dimensional collision avoidance is accomplished by the PNCAG law. Determination of a collision avoidance vector in

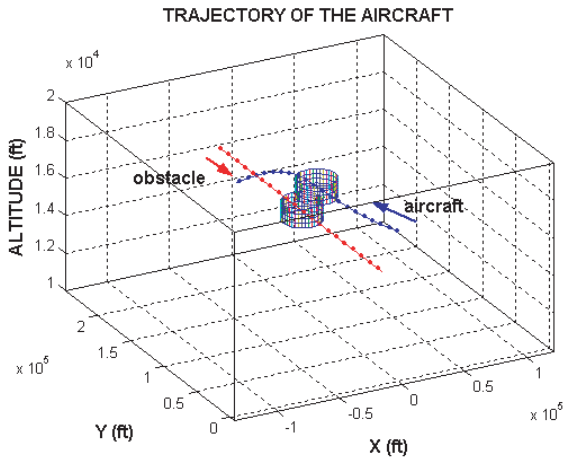

Fig. 18. 3-dimensional simulation results for Case II ($alt_{max} = 6080m$, $alt_{min} = 3048m$ $\eta_U = 1.7966$, $\eta_D = 1.1078$).

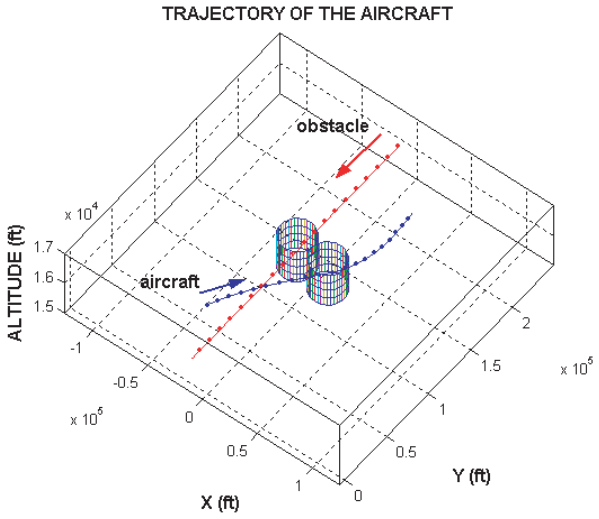

Fig. 19. 3-dimensional simulation results for Case II ($alt_{max} = 5182m$, $alt_{min} = 4572m$, $\eta_U = 17.0$, $\eta_D = 17.0$).

conjunction with a weighting parameter to adjust maneuver directions allows us to design the desired avoidance maneuvers.

7. CONCLUSIONS

A collision avoidance guidance law motivated by the conventional proportional navigation guidance method is applied successfully to the collision avoidance of aircraft. The proposed guidance law was tested through stability analysis and simulation study. From the simulation results, the new approach effectively achieves collision avoidance against the target aircraft with different initial conditions. The three-dimensional collision avoidance guidance law was also verified through simulation. By simple geometric analysis, the collision avoidance vector was shown to be uniquely determined. The aircraft velocity vector was also steered toward designed points of the safety boundary in the three-dimensional formulation. The weighting parameter for vertical maneuver enables us to design avoidance maneuvers in either vertical or horizontal directions with the same initial conditions.

APPENDIX A

In this appendix, the kinematic relationship for the collision avoidance angle in (2) is derived. First, Fig. A.1 shows the angle variables defined to assist the mathematical derivation.

In Fig. A1, the angle variable ϕ satisfies

$$sin\phi = \frac{y}{R_T}, \quad cos\phi = \frac{x}{R_T}. \tag{A1}$$

Differentiation of (A1) yields

$$cos\phi\dot{\phi} = \frac{\dot{y}R_T - y\dot{R}_T}{R_T^2} = \frac{\dot{y}}{R_T} - \frac{\dot{R}_T}{R_T} sin\phi. \tag{A2}$$

Thus,

$$\dot{\phi} = \frac{\dot{y}}{R_T cos\phi} - \frac{\dot{R}_T}{R_T} tan\phi. \tag{A3}$$

Since $\dot{y} = -v_{rel} sin\psi_{rel}$, (A3) can be rewritten as

$$\dot{\phi} = -\left(\frac{v_{rel} sin\psi_{rel}}{R_T cos\phi} + \frac{\dot{R}_T}{R_T} tan\phi \right). \tag{A4}$$

Similarly, for the angle variable γ, it can be shown that

$$sin\lambda = \frac{R_P}{R_T} \tag{A5}$$

and

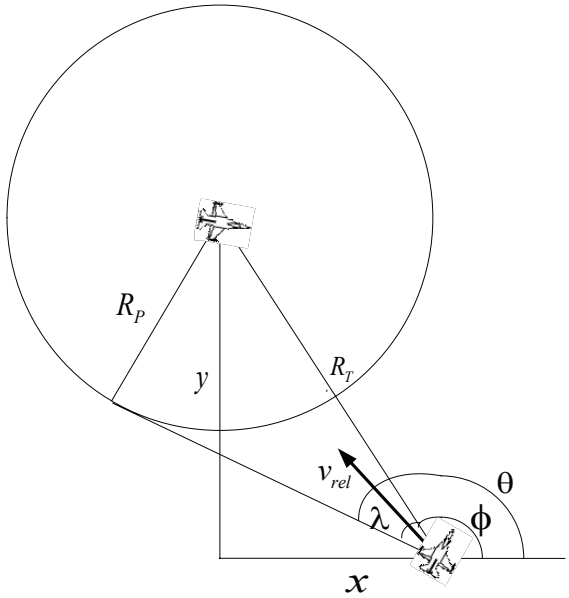

Fig. 20. Angle variables to define the kinematic relationship.

$$cos\lambda\dot{\lambda} = -\frac{\dot{R}_T}{R_T} sin\lambda \tag{A6}$$

thus

$$\dot{\lambda} = -\frac{\dot{R}_T}{R_T} tan\lambda. \tag{A7}$$

Finally, by using $\dot{\theta} = \dot{\phi} + \dot{\lambda}$, one can derive the kinematic equation for the angle variable θ as (2).

$$\dot{\theta} = -\left[\frac{v_{rel} sin\psi_{rel}}{R_T cos\phi} + \frac{\dot{R}_T}{R_T}(tan\phi + tan\lambda) \right]. \tag{A8}$$

APPENDIX B

Since $t_{go} \in [0, t_f]$ is positive, supplementary statements are necessary to prove $c_1 + c_2 / t_{go}$ is positive also over $t_{go} \in [0, t_f]$. Thus, the following conditions should hold

1) constant c_2 must have a positive value,
2) $c_1 + c_2 / t_f$ must be positive.

Proof 1: Since

$$c_2 = \frac{1}{\Gamma}\left[1 - \frac{2R_p\gamma_0}{R_0} \frac{N-3}{(N-1)^2} \right] \tag{B1}$$

a) If $N \le 3$, then c_2 has a positive value.

b) If $N > 3$ with $R_0 \gg R_p, \gamma_0$ is small and $(N-1)^2 > (N-3)$, then it can be regarded that $c_2 \simeq 1/\Gamma$. In addition, $\Gamma > 0$, therefore c_2 is greater than zero.

According to a) and b), c_2 is always positive.

Proof 2: Note that

$$c_1 + \frac{c_2}{t_f} = \frac{v_{rel}}{R_0}\left[1 + \frac{2R_P\gamma_0}{R_0} \frac{2N-3}{(N-1)^2} \right], \tag{B2}$$

(B2) is positive if N is greater than 1.5.

According to Proofs 1 and 2, $c_1 + c_2 / t_{go}$ remains always positive in $t_{go} \in [0, t_f]$ if $N > 1.5$.

REFERENCES

[1] O. Khatib and Burdick, "Motion and force control of robot manipulators," *Proc. of IEEE Robotics and Automation*, pp. 1381-1386, 1986.

[2] P. Tang, Y. Yang, and X. Li, "Dynamic obstacle avoidance based on fuzzy inference and principle for soccer robots," *Proc. of IEEE 10th International Conference on Fuzzy Systems*, vol. 3, pp. 1062-1064, 2001.

[3] D. Rathbun, D. S. Kragelund, A. Pongpunwattana, and B. Capozzi, "An evolution based path planning algorithm for autonomous motion of a UAV through uncertain environments," *Proc. of IEEE Digital Avionics Systems Conferenc*, vol. 2, pp. 8 D2-1-8D2-12, 2002.

[4] C. Tomlin, G. Pappas, and S. Sastry, "Conflict resolution for air traffic management: a study in multi-agent hybrid systems," *IEEE Trans. on Automatic Control*, vol. 43, no. 4, pp. 509-521, 1998.

[5] K. Sigurd and J. How, "UAV trajectory design using total field collision avoidance," *Proc. of AIAA Guidancee, Navigation, and Control Conference*, 2003.

[6] A. Ryan, M. Zennaro, A. Howell, R. Sengupta, and J. Hedrick, "An overview of emerging results in cooperative UAV control," *Proc. of 43rd IEEE Conference on Decision and Control, Atlantis*, Paradise Island, Bahamas, pp. 602-607, 2004.

[7] A. Chakravarthy and D. Ghose, "Obstacle avoidance in a dynamic environment: a collision cone approach," *IEEE Trans. on Systems, Man and Cybernetics - Part A: Systems and Human*, vol. 28, no. 5, pp. 562-574, 1998.

[8] J. Ben-Asher, I. Yaesh, *Advances in Missile Guidance Theory*, AIAA, 1998.

[9] G. Vachtsevanos, L. Tang, and J. Reimann, "An intelligent approach to coordinated control of multiple unmanned aerial vehicles," *American Helicopter Society 60yr Annual Forum*, Baltimore, MD, June 7-10, 2004.

[10] D. E. Chang, S. C. Shadden, J. E. Marsden, and R. Olfati-Saber, "Collision avoidance for multiple agent systems," *Proc. of the 42nd IEEE Conference on Decision and Control*, Maui, Hawaii, USA, December, 2003.

[11] J. How, E. King, and Y. Kuwata, "Flight demonstration of cooperative control for UAV teams," *Proc. of AIAA 3rd "Unmanned Unlimited" Technical Conference, Workshop and Exhibit*, Chicago, IL, September 20-23, 2004.

[12] A. Stephen, Murtaugh, E. C. Harry, "Fundamentals of proportional Navigation," *IEEE Spectrum*, pp. 75-85, 1966.

[13] B. A. Kumar and D. Ghose, "Radar-assisted collision avoidance/guidance strategy for planar flight," *IEEE Trans. on Aerospace and Electronic Systems*, vol. 37, no. 1, pp. 77-90, 2001.

[14] C. D. Yang and C. C. Yang, "Optimal pure proportional navigation for maneuvering targets," *IEEE Trans. on Aerospace and Electronics Systems*, vol. 33, no. 3, pp. 949-957, 1997.

[15] P. Gurfil, M. Jodorkovsky, and M. Guelman, "Finite time stability approach to proportional navigation systems analysis," *Journal of Guidance, Control, and Dynamic*, vol. 21, no. 6, pp. 853-861, 1998.

[16] Y. Watanabe, A. J. Calise, and E. N. Johnson, "Vision-based obstacle avoidance for UAVs," *AIAA Guidance, Navigation, and Control Conference and Exhibit*, Hilton Head, SC, USA, August 2007.

[17] B. A. Kumar, B. A. and D. Ghose, "A proportional navigation based collision avoidance/guidance strategy for low-altitude flight," *Proc. of the 3rd Asian Control Conferenc*e, Shanghai, China, pp. 171-176, July 2000.
[18] A. Sarka, P. Tiwari, S. Srinivasan, R. Bhattacharjee, and D. Ghose, "Generalized PN guidance law for a practical pursuer evader engagement," *Proc. of AIAA Guidance, Navigation, and Control Conference, and Exhibit*, 2003.
[19] P. F. Curran, "Proof of the circle criterion for state space systems via quadratic lyapunov function-part I," *International Journal of Control*, vol. 57, no. 4, pp. 921-955, 1993.
[20] P. F. Curran, "Proof of the corcle criterion for state space systems via quadratic lyapunov function-part II," *International Journal of Control*, vol. 57, no. 4, pp. 957-969, 1993.
[21] P. Zarchan, *Tactical and Strategic Missile Guidance*, AIAA Education Series, AIAA Inc, fourth edition, 1994.
[22] C. K. Ryoo, H. Cho, and M. J. Tahk, "Closed-form solution of optimal guidance with terminal impact angle constraint," *Proc. of IEEE Conference on Control Applications*, Istanbul, Turkey, vol. 1, pp. 504-509, 2003.

Su-Cheol Han received the B.S. degree from Korea Airforce Academy, Korea, in 1997, and the M.S. degree from Korea Advanced Institute of Science and Technology, Korea, in 2005. At present, he is serving as a pilot in Korea Airforce. His research interests are UAV guidance and control, especially collision avoidance.

Hyochoong Bang received the B.S. and M.S. degrees in aeronautical engineering from Seoul National University in 1985 and 1987, respectively. He also received the Ph.D. degree in 1992 from Texas A&M University. From 1992 to 1994, he worked as a Research Assistant Professor at the U.S. Naval Postgraduate School (NPS) conducting spacecraft attitude control research. From 1995 to 1999, he worked for Korea Aerospace Research Institute. Since 2001 he has been a Professor at Korea Advanced Institute of Science and Technology. His current research interest include spacecraft attitude control, spacecraft guidance, UAV guidance and control.

Chang-Sun Yoo received the B.S. degree from Korea Aerospace University, Korea, in 1987, the M.S. degree from Korea Advanced Institute of Science and Technology, Korea, in 1991 and the Ph.D. degree from Chungnam National University, Korea, in 2003. Since 1991, he has been a Research Engineer in Korea Aerospace Research Institute, Korea. His research interests are flight simulation, flight control system, inertial and GPS navigation.